Combust. Sci. and Tech., 1994, Vol. 97, pp. 315–330
Photocopying permitted by license only

Heat Release Rate and Induced Wind Field In a Large Scale Fire

T. OHLEMILLER and D. CORLEY *Building and Fire Research Laboratory, National Institute of Standards and Technology*

(Received July 9, 1993; in final form Oct. 26, 1993)

ABSTRACT— Logging slash on a 486 hectare site in Ontario was burned as part of a Forestry Canada forest management program. A 100 hectare portion of this site was instrumented by several groups interested in large scale fires. NIST utilized Forestry Canada data on mass loading before and after the fire, total burning area as a function of time and burning duration to estimate the spatial and temporal pattern of heat release during the burning of the instrumented section of the fire. The heat release rate was estimated to reach $2–4 \times 10^7$ kW during the time of interest. This information was utilized in the context of a flow model due to Baum and McCaffrey to calculate the near-ground flow field induced by this heat release pattern; the results compared moderately well with point measurements made in the field.

Key Words: Forest fires, fire-induced winds, flow model, heat release rate

INTRODUCTION

Forestry Canada routinely conducts large scale burns of areas of forest which have been logged. These burns clear the area for replanting of trees. The logged area typically has been stripped of all valuable timber but retains some mature standing trees of no commercial value plus logging slash (tree pieces of various sizes from all species growing on the site), immature specimens of all species, a wide variety of brush and the decayed detritus layer on the forest floor (duff). This array of fuel is inherently spatially non-uniform though the practice of "tramping" (systematic compaction of the fuel with a bulldozer) improves this somewhat.

The Defense Nuclear Agency sponsored the participation of several organizations in the study of a 486 hectare burn of this type in Hill Township near Chapleau, Ontario. The overall goal was the development of a better level of understanding of large scale fires.

The overall rate of heat release from such a fire drives the flow which supplies air to the fire. This air flow also plays a major role in the rate of flame spread into unburned fuel areas and thus, in turn, influences the rate of heat release. This tight coupling between air flow and heat release must ultimately be unravelled if the nature of large fires is to be fully understood; no tested model of this coupling is available at present. (The very useful forest fire model of Rothermel (1972), for example, predicts fire spread in response to such factors as wind but includes no wind field prediction.) As a first step in this process, it is useful to know if the flow field can be correctly estimated given the overall rate of heat release at any time. It is necessary to know the spatial distribution of this heat release if one is to properly predict the flow field near ground level where it interacts with the fire (Baum and McCaffrey, 1989).

The goal here is then to obtain an estimate of the pattern of heat release at one or more times in the fire that took place in Hill Township. This information is used in the context of a model for multiple interacting plumes (Baum and McCaffrey, 1989) to calculate the near-ground flow field; the result is compared with the flow velocities measured at specific sites during the fire.

COMPONENTS OF THE RATE OF HEAT RELEASE CALCULATION

The rate of heat release from a large tract of logging slash like that burned in this study is dependent on a large number of factors. Among them are the characteristics of the fuel bed (species distribution, size distribution of the twigs and boles, their moisture content, packing arrangement, the quantity of duff and litter), the terrain (departure from flatness), the ambient weather (wind, humidity) and the ignition pattern. In the case of the particular segment of the burn that is the focus in this study (designated as Block A), there is an additional complication brought on by the fact that this was not the first part of the burn area that was ignited. Block A1, immediately adjacent to Block A, was ignited first creating its own wind field which then influenced the burning of Block A. As a mnemonic, the reader may wish to note that the number "1" in A1 stands for "first ignited". Figure 1 shows Block A1 in relation to Block A; the shaded band between these two areas is their approximate dividing line.

The ignition process is carried out from a helicopter which drops an intermittent string of flaming gelled gasoline. The amount of this fuel is negligibly small and the fire

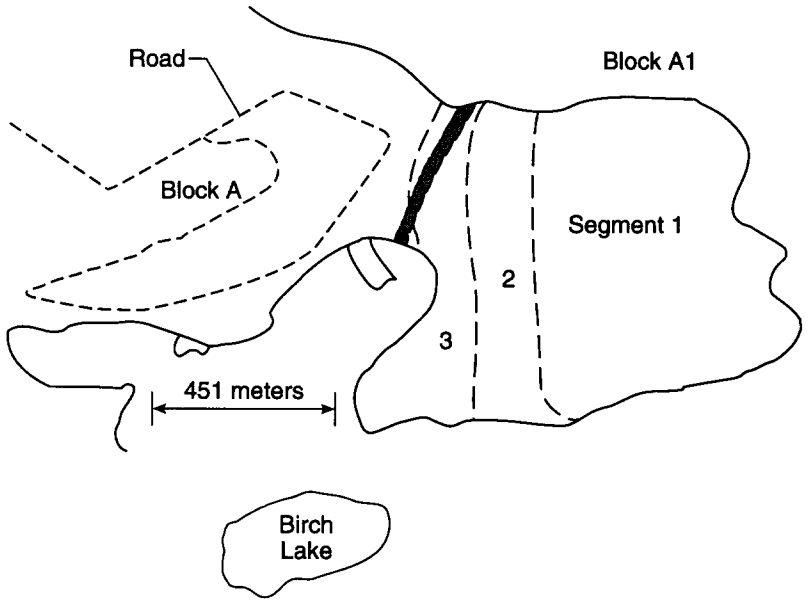

FIGURE 1 Schematic of Block A and Block A1 showing the approximate boundaries used to break Block A1 into three segments based on roughly equal ignition times. Also shown is Birch Lake which was the primary length reference for the NIST analysis of the infrared videotape.

spreads by its own heat release. The ignition process is somewhat protracted, requiring about $\frac{1}{2}$ hour in Block A1, for example.

Calculation of rate of heat release is simple, in principle. It is the product of the rate of mass loss per unit area, the total area undergoing the mass loss and the heat of combustion of that mass. However, wood and the other natural fuels present on the burned area undergo not only flaming but also smoldering combustion; the rates and the reaction heats of these two types of processes differ substantially so that it is necessary to keep track of each area undergoing the two processes separately. It is also necessary to obtain a measure of the two differing rates of these combustion processes.

Most of the field data used in the calculations discussed here comes from Forestry Canada; NIST supplemented their thermocouple measurements to some extent.

The estimation of the various inputs to the rate of heat release calculation will be described only briefly here. Ohlemiller and Corley (1990) give further details and an extensive discussion of the uncertainties. Quintiere (1990) discusses the overall results from all participants in this fire experiment.

Mass Loss Rate Assessment

There is currently no feasible means to directly measure rate of mass loss in the field during a burn. Instead the total mass loss (flaming plus smoldering) is sampled at several locations by a planar intersect technique, well before and well after the actual burn (Brown, 1974). This technique employs well-established correlations between the sizes of wood boles and twigs crossing an arbitrary vertical plane through the fuel bed and the volume distribution of wood present in the sampled region. Sampling at several locations is necessitated by the non-uniform spatial distribution of the logging slash on the burn site. As implemented by Forestry Canada in this study, sampling was done at twelve triangular plots scattered throughout Block A, each thirty meters on a side. The water content of the wood was sampled separately; it varied with the diameter of the wood.

The forest floor is covered by a layer of decaying debris (needles, leaves, twigs) called duff whose density and water content increase with depth. This layer contributes substantially to the net mass loss during the burn, both by flaming and by smoldering. Its mass before and after the burn is assessed by means of layer depth change sampling, done along the sides of the triangles described above. Depth is translated to dry mass per unit area by means of a standard density profile developed by Forestry Canada for the local region. The water content of this duff layer was sampled at two depths.

The results of the above techniques applied to the slash are summarized in Figure 2. One sees that the fire completely consumes all but the largest size class of fuel. These sampling techniques cannot distinguish in which stage of combustion, flaming or smoldering, the mass was lost. The flaming and smoldering mass loss in each size class are apportioned in accord with results from Brown (1972) which is based on two other types of wood (Douglas fir and ponderosa pine versus predominantly spruce and balsam fir here). That reference shows a monotonic decrease in flaming mass loss with increasing fuel diameter, e.g., from 94% for 2 mm diameter twigs to 11% for 3–5 cm diameter branches.

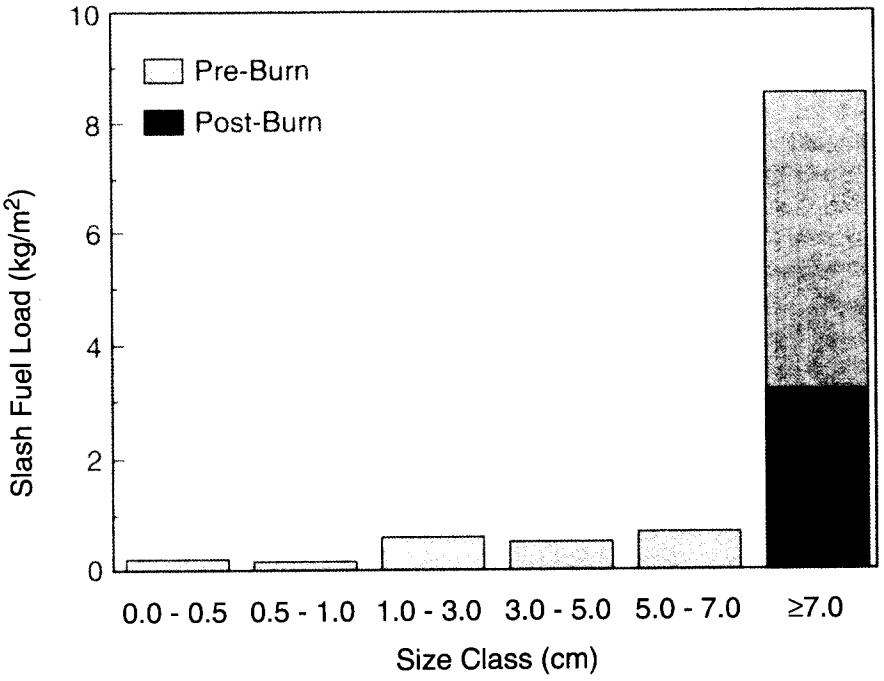

FIGURE 2 Pre- and post-burn slash fuel loadings averaged over all sampling sites.

The result of apportioning flaming and smoldering dry mass loss in this way, when summed over all size classes and averaged over all sampling triangles is

$$\text{flaming: } 0.90 \pm 0.19 \quad (\text{kg/m}^2)$$

$$\text{smoldering: } 6.6 \pm 1.3 \quad (\text{kg/m}^2)$$

Note that there is a surprising dominance of weight loss by smoldering. It is also worth noting that 5.0 of the 6.6 kg/m^2 smoldering mass loss is in the > 7 cm diameter size class. The explanation for this latter result is not clear.

The preceding data on mass loss by the two combustion modes must be coupled with combustion time information in order to infer the rate of each process. Estimating the flaming and smoldering times is difficult at best; see Ohlemiller and Corley (1990) for a detailed discussion. The flaming time was estimated from both thermocouples placed at various points in the sampling triangles and from video tapes taken within the fire. Using these combined data sources, Forestry Canada inferred flaming and smoldering durations of approximately 3 and 22 minutes, respectively (Quintiere, 1990). The present authors, using their own interpretation of very similar data infer an area averaged flaming time of at least 4 minutes. US Forest Service personnel, using an entirely independent technique based on a carbon balance in sampled gases, inferred a flaming time consistent with the two preceding values (Quintiere, 1990). The smoldering times appear quite ambiguous, however; our thermocouples suggest a time comparable to that deduced by Forestry Canada but other features of the fuel bed

consumption (especially the large smoldering mass loss inferred in the largest slash size range) suggest substantially longer times (a factor of two or more). These ambiguities have led us to calculate the heat release rate in more than one way.

The mass loss and burning duration results are used to infer mass loss rate due to both flaming and to smoldering, separately. The simplest way in which to do this is to assume that the rate is constant in a given area for the inferred flaming time and then for the smoldering time. Since the burn area is increasing during the time of interest due to continuing ignition and flame spread, the choice of what area to apply such a concept to is not straightforward. This constant rate idea has been used in the past by McRae and Stocks (1987). On the other hand, Ward and Hardy (1984) found that the mass consumption rate in a series of small, undisturbed test plots (covered with logging slash) exhibited an exponential decay with time after an initial build-up period associated with flame spread. Both of these concepts were utilized in the rate of heat release calculations, in order to test the sensitivity of the results to the mass consumption rate model.

Burning Area Versus Time

The second element in the rate of heat release calculation is the area undergoing a specific combustion process, flaming or smoldering. Recall that our ultimate goal is to calculate the fire-induced flow field and this is affected both by the growing fire in Block A (instrumented block) and the decaying fire in Block A1 (block ignited first). Thus this area information is needed for both blocks of the fire.

In this type of fire, virtually all of the increase of burn area with time is due to the spreading of flames; the fraction of total area that is directly ignited by the helicopter torch is negligibly small.

A Forestry Canada helicopter with a infrared imaging camera provided detailed data on the time-dependent spread of the burn area in Block A, but the data in Block A1 were more sketchy due to limited videotaping over that area. Unfortunately, the camera was unable to differentiate between flaming and smoldering areas. Using a calibration based on the known size of an adjacent lake, one could infer the total burning area at a given time. The differentiation between flaming and smoldering areas (needed in the wind field calculation below) had to be done using the characteristic flaming time mentioned above. Thus, in a given infrared image of the burn, only the new area generated in the preceding 3–4 minutes was taken to be undergoing flaming; the remainder was inferred to be smoldering. This technique also provides the geometric layout of the two types of combustion zones, also needed in the wind field calculations. This technique for separating flaming and smoldering areas is consistent with the concept of characteristic times for each but it is not entirely satisfactory if only a single characteristic time is used for smoldering; this led to the use of two different smoldering times in Model 3 for heat release rate, discussed below.

Figures 3 and 4 show the total burning areas obtained for Block A1 and A, respectively. Recall the former was burning adjacent to the instrumented Block A and thus assists in generating the wind field there. Since the ignition of Block A1 began nearly half an hour before that of Block A, the former was inferred to be essentially only smoldering during the time of interest. Block A1 was divided into three segments, each

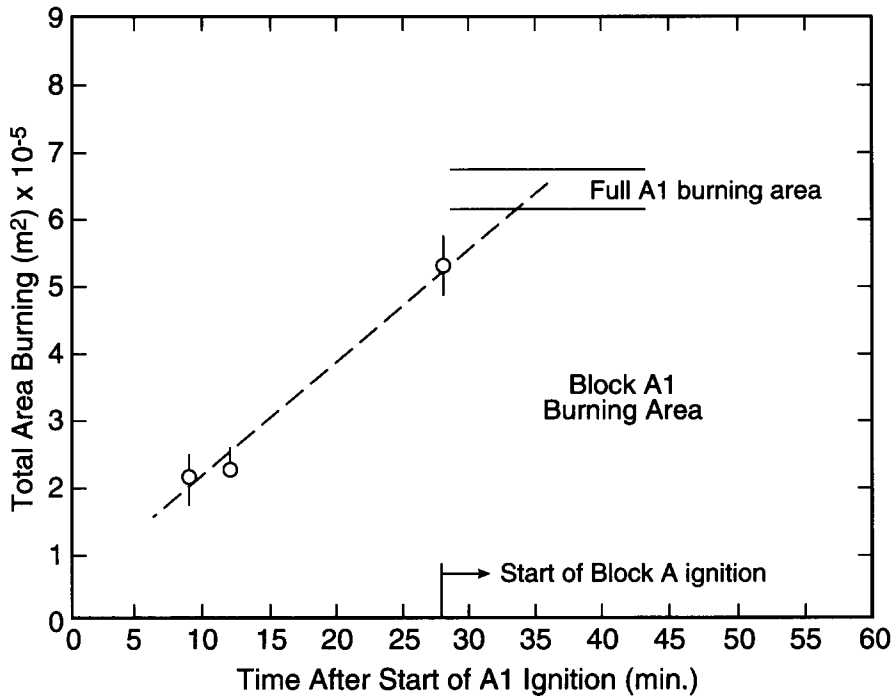

FIGURE 3 Estimated total burning area in Block A1 as a function of time.

of which had nearly the same ignition time throughout that segment, as indicated by the IR camera. The decay of the smoldering heat release there, during the time of interest in Block A, was thus attributed to three distinct spatial areas whose shapes and locations were inferred from the IR camera data (see Figure 1). The Block A heat release pattern was treated with greater precision, as indicated below.

Heats of Combustion

One needs the effective values of flaming and smoldering combustion heats for both the slash and the duff. Since these values are affected by water vaporization, this needs to be accounted for as well.

Samples of the small diameter slash fuels (up to about 1 cm dia.) and of the litter/duff layer were collected on the morning of the burn. The sampling process was not statistically designed to be truly representative but the material did come from several different spots and did include a mix of species.

Measurements of the heats of flaming and smoldering were performed in the NIST Cone Calorimeter facility which employs oxygen consumption as a means of determining the evolved heat. This measurement technique is generally accurate to about $\pm$ 5%. It utilizes the fact that the heat evolved per unit mass of oxygen consumed is constant to within about $\pm$ 5% for most organic materials (Huggett, 1980). When the combustion efficiency is not 100%, as is especially the case for smoldering, a correction is made

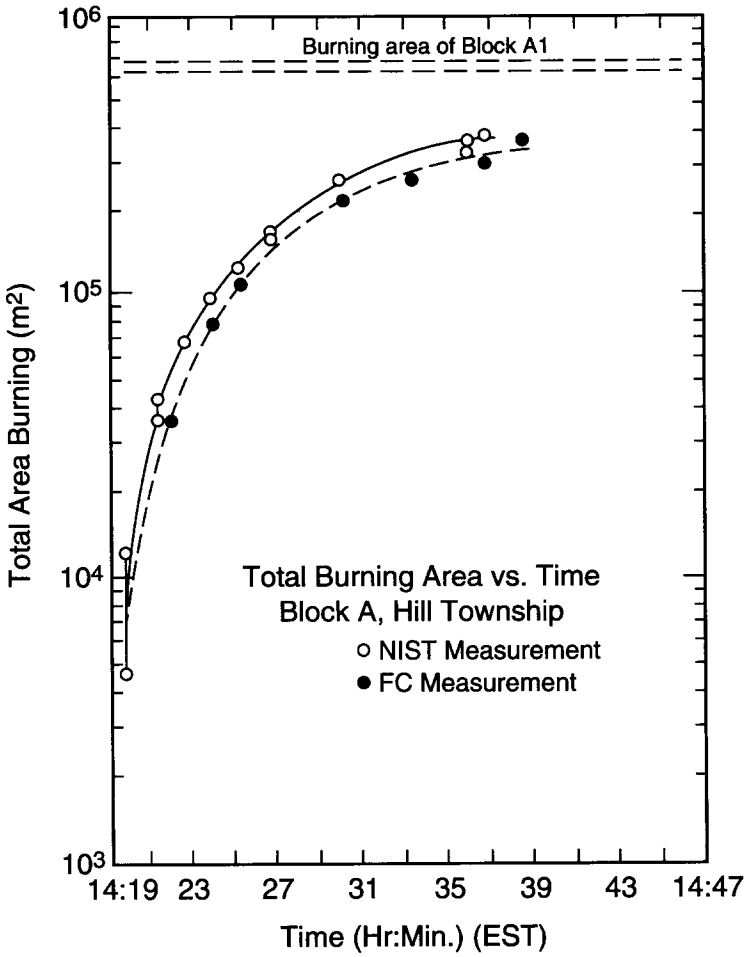

FIGURE 4 Estimated total burning area in Block A as a function of time; results from NIST and Forestry Canada.

based on the amount of CO formed, since its heat evolution per unit mass of oxygen consumed is substantially less than for CO_2. The uncertainties in obtaining and applying these heats to this situation are discussed in Ohlemiller and Corley (1990).

Table I summarizes the results of the NIST measurements of combustion heat. The twigs were tested both with and without an external flux of 2 W/cm^2; this is a level of radiant heat flux that might readily exist in portions of the fuel bed during the prescribed burn. Some enhancement of the combustion heat is seen in the flaming stage when the external flux is present due, presumably, to greater participation in the flaming by the varied fuels in the sample; this enhancement is even greater in the subsequent smoldering stage. The substantially larger heat of combustion for smoldering is consistent with the results of Susott *et al.* (1975); it is a consequence of the high oxygen content of the volatiles burned during flaming as compared to the high carbon

TABLE I
NIST cone calorimeter results for heats of combustion of twig and duff samples

Material	Water Wgt. % of Total	Incident Heat Flux (W/cm^2)	Heat of Flaming Combustion (kJ/g Lost)	Heat of Smoldering Combustion (kJ/g Lost)
Twigs[1]	8.7[2]	0	12.1 ± 1.6[3]	26.6 ± 4.3[4]
"	"	0	12.0 ± 4.5	16.6 ± 1.7
Twigs	8.7	2.0	13.2 ± 1.4	27.4 ± 2.9
"	"	"	13.5 ± 1.4	31.6 ± 5.8
"	"	"	15.0 ± 1.0	32.5 ± 4.4
Duff	7	2.0	14.0 ± 2.2[5]	$7.2 \rightarrow 9.0$ (incr. w. time)
"	"	"	12.8 ± 1.4	$6.6 \rightarrow 11.0$ (incr. w. time)
"	"	"	13.0 ± 1.4	$6.7 \rightarrow 7.1$ (incr. w. time)
Duff	25	2.0	No flames	5.0 ± 0.5
"	"	2.0	"	5.7 ± 0.6
"	"	"	"	5.7 ± 0.6
Duff	50	2.0	No flames	2.2 ± 0.2

[1] Random mix of species, sizes generally 1–10 mm dia
[2] In equil. w. 50% R. H. at 21°C; expressed as wgt. % of (water and wood) weight
[3] Avg'd over 60 sec. period after ignition
[4] Avg'd over 60 sec. period subsequent to flame extinction
[5] Avg'd over 30 sec. period after ignition

content of the char consumed during smoldering. In utilizing these results, values with and without external flux are averaged together, since both situations undoubtedly existed on the burn site (though the proportion of each is impossible to estimate). The duff/litter material, when it flamed, had a quite similar heat of flaming to that of the woody material. Interestingly, however, it would only flame when it was nearly dry and was subjected to an external heat flux. When the water content was higher, the only response was smoldering.

In contrast to the heat of smoldering for the twigs, that of the duff is much lower and the net value decreases strongly with water content of the duff. Since flaming prior to smoldering was minimal or absent, the smoldering process here is consuming the original, highly oxygenated fuel, not a carbonaceous char. The combustion efficiency is also reduced; the CO production is as much as a factor of ten higher than during the flaming combustion of the twigs. After correcting for water content, the values from the 7 and 25% water duff material were averaged and used in the calculations below.

It was noted above that the water content of the fuel influences the net heat evolved from each burning process and that this must be accounted for in our final assignment of reaction heats. The water contents of the fuels before the burn were determined; the post burn water content was estimated using rough calculations of the thermal wave penetration during the burn for various fuel dimensions (Ohlemiller and Corley, 1990). A mass weighted average of the heat of water vaporization together with the dry fuel heats of combustion was used to obtain an estimate of the net heats of combustion.

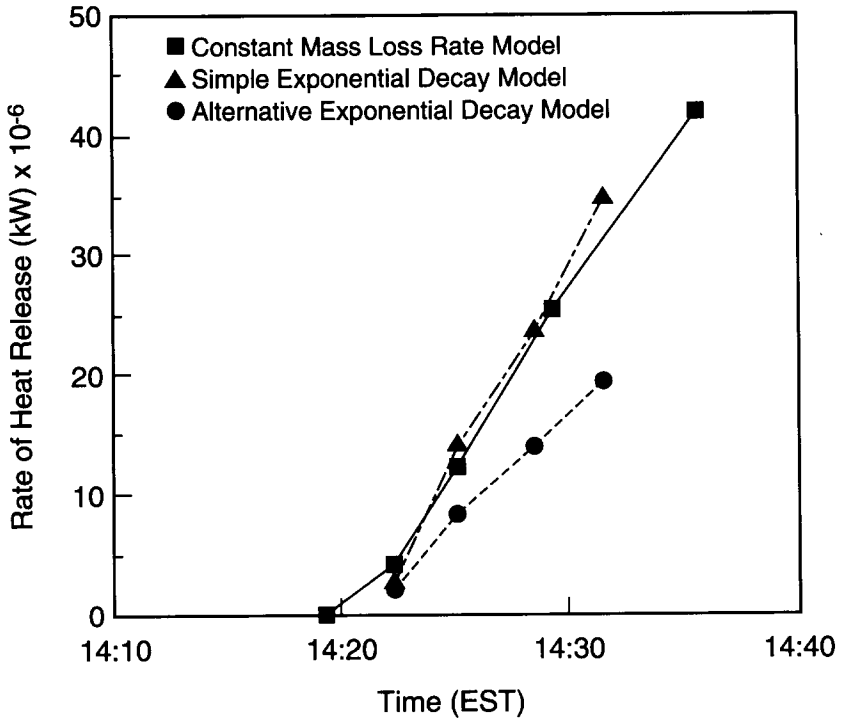

FIGURE 5 Total rate of heat release in Block A as a function of time (EST). Estimates shown are based on three differing models of the time dependence of the local mass burning rate.

CALCULATION OF HEAT RELEASE RATE

Because of ambiguities in the behavior of the fuel, particularly with regard to flaming and smoldering durations, the heat release calculations were carried out in accord with three differing sets of assumptions.

Model 1 Assumes that flaming and smoldering occur at constant rates in distinct succession at any location, each with its own characteristic time.

Model 2 Assumes that both flaming and smoldering decay exponentially subsequent to ignition at any location with smoldering being initiated one characteristic flaming time after flaming itself starts.

Model 3 Is an elaboration of Model 2 in which separate time constants are used for the flaming and smoldering of slash fuel above and below a 7 cm diameter cutoff.

Model 1 incorporates the simplest possible assumptions as to fuel behavior. Such a model has been used previously to make heat release rate estimates (McRae and Stocks, 1987; McRae, 1986). The exponential decay behavior employed in the two more elaborate models is based on experimental results described in Ward and Hardy (1984). The exponential dependence extends the heat release process relative to the constant rate assumed in Model 1 with the result that, at any time, the total heat release rate is

generally less. In Model 3 longer time constants are applied to the large diameter fuel boles with the result that the total instantaneous heat release rate is lowered still further than the value found with Model 2. This is done to bring the large fuel behavior more into accord with the authors' experience.

All three of these models are discussed in detail in Ohlemiller and Corley (1990). Here we simply indicate the total heat release rate from each at early times in the ignition of Block A; see Figure 5. One sees there that the net impact of the differing model descriptions is at most a factor of two in overall heat release rate. Quintiere (1990), which summarizes the data from all participants in this mass fire experiment, shows that Forestry Canada and the US Forest Service obtained comparable estimates of the overall heat release rate in this time interval.

The wind field calculations below used the heat release estimates obtained via Model 2. In doing this, one accounts not only for the total heat release rate but also its spatial distribution at each calculation time, in accord with the model assumptions. Thus there are three types of burning area to be separately accounted for: 1) the area ignited into flaming alone during the last characteristic flaming time period (3 minutes); 2) the area where smoldering was just initiated (and flaming continues, though it has had more than three minutes to decay); 3) all of the remaining area, where smoldering and flaming continue to decay, having been initiated more than three and six minutes previously, respectively. The shapes and locations of each of these areas are inferred from the infrared video tapes of the fire by examining the detailed change in shape of the burning area at three minute intervals.

PREDICTION OF WIND FIELD

As noted, the rate of heat release results from Model 2 have been used in an effort to calculate the near-ground flow field that they produce. The predictions are compared with the wind velocity vectors measured at specific sites in Block A (the instrumented block). The measured values come from Forestry Canada cup anemometers ten meters above the ground and are believed to have good accuracy ($\pm$ few percent) up to the time the fire reached their location. The velocity and wind direction data were noisy due to turbulence and thus were averaged over a three minute interval around the time of use. Since the ground in Block A had height variations of the order of $\pm$ 15 m, the ambient wind varied from point to point; this was accounted for by using local fifteen minute averages of the pre-fire wind to estimate the ambient wind vector contribution during the fire.

The flow model used is that due to Baum and McCaffrey (1989). This model treats the large fire as a collection of individual, radially symmetric fires which are to be placed spatially in accord with the burn patterns obtained from the infrared video tape. If this can be done successfully then the model should describe the flow field both within the fire array and distant from it.

Baum and McCaffrey hypothesized that any mass fire would necessarily yield a large array of relatively small plumes rather than a single large plume. Heskastad (1991) demonstrated in a reduced-scale experiment that plume break-up over a uniform fuel array will occur if the heat release rate per unit area divided by the square root of the

array diameter falls below a certain value. In the time interval of interest the fire in Block A falls below this limit by an order of magnitude. However, the existence here of an array of plumes rather than a single plume is more clearly attributable to the spotty manner in which the fire was ignited, coupled to the non-uniformity of the fuel bed on a scale of the order of ten meters or so.

Applying this model here is not as simple as one might hope. There are two complicating factors. First, the model is sensitive to the actual number of individual fire plumes. This is not an artifact of the model but rather reflects the total plume "surface area" available for entraining surrounding air. The greater this number, the greater the net induced flow velocity because the total entrainment by the plumes increases. However, the infrared camera data discussed above do not provide clear-cut information on the number of plumes above any given burning area. Comparisons between visible photos and the infrared tape suggest that individual burning areas on the periphery of the fire yield distinct plumes but that, as one proceeds toward the center of the fire, plumes from more than one area rapidly merge to become one effective plume. The lack of any way to quantify this means the number of plumes assigned to Block A at any given time is an estimate with an uncertain accuracy.

The second complication in applying the flow model to this situation derives from the fact that Block A1 was ignited first. It was pointed out above that this Block is effectively undergoing only smoldering combustion in the time interval of interest here for Block A (the instrumented block). Estimates were made of the rate of heat release from this smoldering and it was noted that Block A1 apparently dominates over Block A until a time of 14:25 (EST) or later. Unfortunately, this is the time interval when the model comparison is to be made. The induced flow from Block A1 must be part of the flow field calculation, therefore. However, the Baum and McCaffrey model is based on the structure of a flaming fire plume. There is no comparable information available for the structure of a plume over a smoldering area, particularly an area like that which Block A1 presents in this time interval — a 60 hectare fuel bed that is smoldering with an unknown degree of spatial uniformity.

To deal with this second complication, the description of Block A1 was adjusted, in the time before the Block A heat release rate was significant, in an attempt to obtain the experimentally measured velocities at the anemometer positions. The ambient wind field tends to dominate and obscure the Block A1 fire effects at most of these locations; the ambient wind was added vectorially to the velocity values predicted by the model. The added values were the average values computed at each anemometer position for the fifteen minutes prior to the start of ignition in Block A1. Adjustment of the Block A1 description called for modifying the number and strength of the flaming plume-like fires assigned to the three segments of this Block within the constraint that each segment have the total energy release rate computed for it. The actual locations of these fires within the confines of each segment of Block A1 were randomly assigned. Clearly this heuristic procedure precludes any possibility of accurately modeling the wind field within Block A1.

The adjusting of the A1 description was done at a time of 14:19. At this time the heat release in Block A (instrumented area) was two orders of magnitude less than that in Block A1 (first block ignited). Figure 6(a, b, c) shows the results of successive descriptions of the Block A1 heat release distribution. Note that the description of the shape of

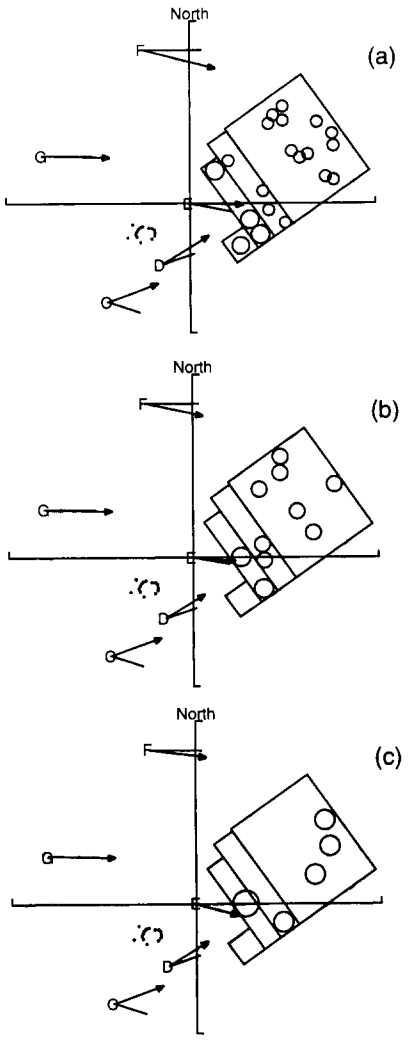

FIGURE 6 Comparison of calculated (line with arrow head) and measured (line without arrow head) velocity vectors at Forestry Canada anemometer locations at 14:19:20 (EST). Description of Block A1 is being varied in (a), (b), and (c) to improve velocity vector matching. Version (c) is used for model calculations at next two times.

Block A1 has been approximated by a series rectangles. The small area ignited in Block A at this time is visible in this scaled diagram as a ring of small circles. In Block A1, each circle's fraction of the total circle area is proportional to the fraction it represents of the total Block A heat release rate at this time. The arrows showing the experimental and calculated wind velocity vectors are positioned with their origins at the anemometer locations. The line having half an arrow head at each anemometer location is the wind

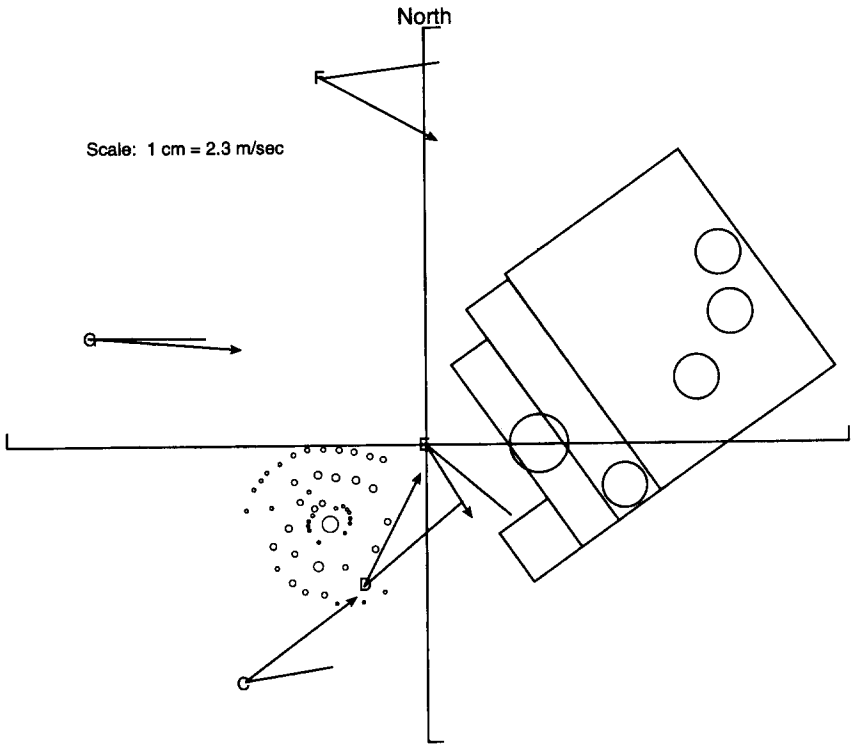

FIGURE 7 Comparison of calculated and measured velocity vectors at Forestry Canada anemometer locations at 14:22:24 (EST).

vector calculated from the model; the other line at each point is the measured wind vector at 14:19:20. Examination of Figure 6 reveals that the best agreement between model and experiment at the five anemometer positions was obtained by having only five fires in Block A1 (all three cases shown in Fig. 6 have the same total heat release rate); as the number of fires was increased the predicted magnitudes of the velocity vectors tended to become substantially larger than the measured values. This best description of Block A1 was then retained for the model calculations at two further times; the total heat release rate in A1 was allowed to decay in accord with the calculations indicated above.

As the fire grows in Block A, the proper description of it for the model (i.e., the number of plumes it is composed of) is problematical, as indicated above. As a first attempt, this fire was described by a large number of small circular fires located so as to give very close conformance to the actual fire outline seen in the infrared video pictures. This emphasis on fire shape ignored the fact that the model predicts increasing total entrainment as the number of fires increases (for the same value of total heat release rate); the resulting values of predicted wind velocity were much too high. Subsequently the total number of fires was reduced in accord with the indication, mentioned above,

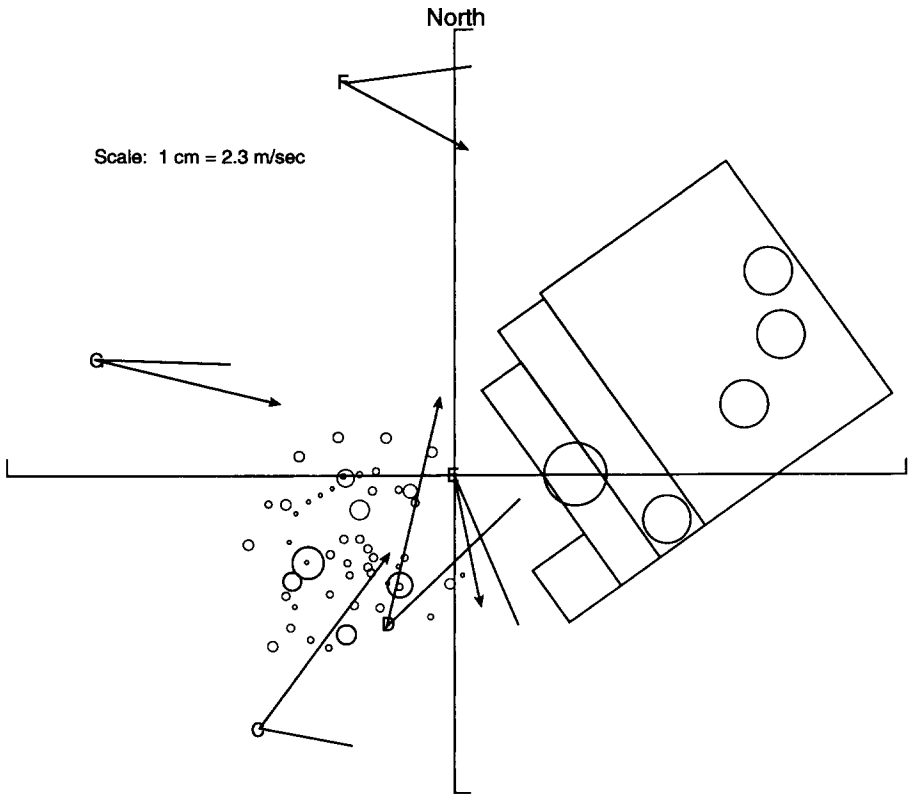

FIGURE 8 Comparison of calculated and measured velocity vectors at Forestry Canada anemometer locations at 14:25:05 (EST).

that the plumes appear to merge as one moves toward the center of the Block A fire. This resulted in a factor of four reduction in the number of plumes with some compromise as to the exact placement of the center of each plume relative to the real fire. (The coordinates of each plume are measured on a scaled map so that their position relative to the anemometers and to Block A1 can be correctly determined.) This uncertainty in placement can be expected to somewhat degrade the accuracy of predictions as to wind vector direction close to the fire.

Figures 7 and 8 show the heat release patterns inserted into the model at 14:22:24 and 14:25:05, respectively. The pattern at 14:22 involved a fairly accurate assignment of a reduced number of fire plumes to the pattern revealed in the infrared video tape at this time; the pattern at 14:25 was deduced in a somewhat cruder fashion by lumping together successive groups of four fires from a spatially accurate description with a large number of fires.

Examination of these two Figures shows that the model does a fairly good job of predicting the magnitude of the velocity vectors; only location C is off by a factor of two by 14:25. The model also seems to overestimate the shift in velocity vector orientation. Both the over-prediction of velocity magnitude and velocity orientation shift may be

due, at least in part, to the fact that the model is steady state, as employed here. The overall fire in Block A is growing very rapidly and the flow field may require a few minutes to adjust; thus the actual flow field would lag the steady flow field accompanying any given pattern of heat release by a few minutes. Of course the ambiguities, mentioned above, in applying this model to this difficult situation may also be at the heart of what appears to be an increasing difference between model and experiment as time progresses.

CONCLUDING REMARKS

Accurate estimation of the overall rate of heat release from a large scale fire is a very challenging undertaking. While estimates have been produced here which fall in a fairly narrow band (factor of two), the true precision of these values cannot presently be determined. Ohlemiller and Corley (1990) give a brief discussion of possible ways to lessen the principal sources of uncertainty in future large scale burns. However, while it is relatively easy in retrospect to suggest improved ways to obtain data for heat release rate estimates, it is another matter to implement them.

While the comparisons here between predicted and measured flow velocities are fairly successful, it is clear that a really critical test of the Baum/McCaffrey model of induced winds was not possible in the context of this experiment. In fact, this type of experiment (prescribed forest burn) is not well-suited to testing this model. Even if Block A1 had not been ignited first, there would remain the major uncertainties of how to estimate the number of fire plumes driving the flow and how to handle the smoldering portion of the fuel bed that results from the relatively slow ignition process. In addition there is the unknown influence of the uneven terrain which the model does not include and, of course, the substantial uncertainties in estimating the rate of heat release. A scaled down version of a Project Flambeau fire (Palmer, 1981) or a well-defined set of liquid pool fires would be a better context for testing the flow model of Baum and McCaffrey and clarifying the underlying mechanisms for fire-induced winds.

ACKNOWLEDGEMENTS

This work was sponsored by the Defense Nuclear Agency. The authors would like to acknowledge helpful discussions with Howard Baum regarding the flow field calculations. William Rinkinen and Darren Lowe were very helpful in the field study aspects of this work as was Ms. Robin Breese in the post-test data reduction.

Forestry Canada personnel were extremely helpful throughout this project; the authors are particularly grateful to Doug McRae and Chuck Ogilvie.

REFERENCES

Baum, H. and McCaffrey, B. (1989). *Fire Safety Science—Proceedings of the Second International Symposium*, Hemisphere Publishing, Washington, D. C., pp. 129–148.

Brown, J. (1974). "Handbook for Inventorying Downed Woody Fuel", USDA Forest Service General Technical Report INT-16.

Brown, J. (1972). "Field Test of a Rate-of-Fire-Spread Model in Slash Fuels", USDA Forest Service Research Paper INT-116.

Huggett, C. (1980). *Fire Mater.*, **4**, p. 61.
McRae, D. and Stocks, B., "Large Scale Convection Burning In Ontario", Ninth Conference on Fire and Forest Meteorology, April, 1987.
McRae, D., *The Forestry Chronicle*, April, (1986), pp. 96–100.
Ohlemiller, T. and Corley, D., "Estimation of the Rate of Heat Release and Induced Wind Field in a Large Scale Fire", National Institute of Standards and Technology NISTIR 4430, October, 1990.
Palmer, T. Y. (1981). "Large fire winds, gases and smoke", *Atmospheric Environment*, **15**, No. 10/11, p. 2079.
Quintiere, J., "Canadian Mass Fire Experiment", National Institute of Standards and Technology NISTIR 4444, November, 1990.
Rothermel, R., "A Mathematical Model for Predicting Fire Spread in Wildland Fuels", USDA Forest Service Research Paper INT-115, 1972.
Susott, R., DeGroot, W. and Shafizadeh, F., *J. Fire Flamm.*, **6**, July, 1975, pp. 311–325.
Ward, D. and Hardy, C., "Advances in the Characterization and Control of Emissions from Prescribed Fires", Seventy-Seventh Annual Meeting of the Air Pollution Control Association, June, 1984.